Iranian Journal of Science and Technology, Transactions of Civil Engineering (2022) 46:4689–4704
https://doi.org/10.1007/s40996-022-00919-5

RESEARCH PAPER

Experimental and Numerical Investigation of the Flood Waves due to Partial Dam Break

Ayşegül Özgenç Aksoy[1] · Mustafa Doğan[1] · Semire Oğuzhan Güven[1] · Görkem Tanır[1] · Mehmet Şükrü Güney[2]

Received: 19 November 2021 / Accepted: 26 June 2022 / Published online: 20 July 2022

Abstract

The potential destruction of dams is a serious danger for the settlements. Dam break events cause serious loss of life and property in the region, regardless of the reason. The time required to give warn the people of the region is very short since floods develop suddenly during dam breaks. For this reason, the investigation of the flood wave propagation that will occur at the time of possible collapse is important for the emergency action plans to be prepared. In this study, the dam break experiments were carried out in the distorted physical model of the Urkmez Dam and at its downstream part also involving the vegetation. The horizontal and vertical scales are 1/150 and 1/30, respectively. The water depths and local velocities were measured by means of elaborated devices, and the propagation of the flood wave was recorded by high-precision cameras. In addition, numerical analysis was achieved by using the FLOW-3D program. According to the results, it is concluded that as the water level decreases, the time to reach the measurement points of the flood increases and the spatial distribution is delayed. The computed values obtained from the numerical model simulated by using the dam reservoir are in better agreement with those obtained from experiments than those calculated by using the outlet hydrograph.

Keywords Dam break · Vegetation effect · Flow-3D · Flood wave propagation · Distorted physical model

1 Introduction

Dams have very important role for societies due to their functions. The potential destruction of dams is a serious danger for the settlements. Dam break events cause serious loss of life and property in the region, regardless of the reason. The time required to give warn the people of the region is very short since floods develop suddenly during dam breaks. For this reason, the investigation of the flood wave propagation that will occur at the time of possible collapse is important for the emergency action plans to be prepared.

Lauber and Hager (1998) observed the wave velocities and water surface profiles that occurred after the dam broken. In the experiments, the demolition of the dam was modelled in a horizontal rectangular channel. The channel has a length of 14 m and a width of 0.5 m. Measurements were taken with the help of particle image velocimetry (PIV) and camera images. Soares-Frazão (2007) measured the water depths of flood that occurred as a result of collapse by conducting dam break experiments in a channel with a length of 5.6 m and a width of 0.5 m. During experiments, water depths were determined with water level indicators and digital camera. Soares-Frazão and Zech (2008) investigated how settlements will be affected by flood by creating a flood wave in a rectangular channel 36 m long and 3.6 m wide. They compared the measured water velocities and water depths with those obtained by numerical analysis. Froehlich (2008) obtained expressions about the mean breach width, the side-slope ratio of the trapezoidal opening, and the breach formation times with the data obtained from 74 dam failures that had occurred before. The obtained statistical findings were

✉ Semire Oğuzhan Güven
semireoguzhan@gmail.com

Ayşegül Özgenç Aksoy
aysegul.ozgenc@deu.edu.tr

Mustafa Doğan
mustafa.dogan@deu.edu.tr

Görkem Tanır
gorkemtnr@gmail.com

Mehmet Şükrü Güney
sukru.guney@ieu.edu.tr

[1] Department of Civil Engineering, Dokuz Eylul University, Tinaztepe Campus, 35160 Buca, Izmir, Turkey

[2] Department of Civil Engineering, Izmir University of Economics, 35330 Balçova, Izmir, Turkey

applied to the Monte Carlo simulation and used to estimate the uncertainty of peak flows and water levels. Erpicum et al. (2010) investigated the flow formed after the dam break using the method of finite volumes with two-dimensional. They used the shallow water equations in the numerical analysis method. They conducted experiments in physical model to compare numerical data. They obtained coherent results in comparison of numerical and experimental findings. Ozmen-Cagatay and Kocaman (2010) conducted dam demolition experiments in a horizontal rectangular channel. They compared their experimental results with those obtained from the FLOW-3D program using RANS (Reynolds-averaged Navier–Stokes) equations combined with k–ε turbulence model and the SWE (shallow water equations). They showed that the results of both approaches were compatible with their experimental findings. Jeong et al. (2012) analysed how the residential areas were affected by the flood wave propagation caused by the dam break by numerical analysis methods with three different turbulence models. They compared the findings with two different experimental results in the literature. Güney et al. (2014) conducted dam break experiments in the distorted physical model of the Urkmez Dam, in Izmir. The model having a horizontal scale of 1/150 and a vertical scale of 1/30 includes the dam reservoir, dam body and the settlement region at its downstream. In the experiments, the partial dam break was realized by lifting a trapezoidal or triangular part of the dam body and the sudden collapse was simulated by overturning a rectangular gate. The water depths and velocities of the flood were measured at various locations in the downstream area, and the wave propagation was recorded by means of high-precision cameras. Ozmen-Cagatay et al. (2014) investigated the flood wave and shock waves occurred because of dam break in a horizontal rectangular channel of 8.9 m length and 0.3 m width. Then, they translated the experimental conditions to FLOW-3D software and compared the experimental and numerical results. Wood and Wang (2015) examined the flood wave propagation caused by the dam break in a channel with 90-degree bend experimentally and numerically. Haltas et al. (2016) modelled the flood that will occur in the event of the demolition of the Urkmez Dam by using HECRAS and FLO-2D software. Elkholy et al. (2016) carried out a partial dam demolition experiment in a pool with a reservoir at the upstream side and a sink in the downstream. The reservoir was 4.3 m wide and 3 m long and can take water up to 0.75 m high. Downstream area was 8 m long and 4.3 m wide. Bayon et al. (2016) compared two different computational fluid dynamics (CFD) programs (Flow-3D and OpenFOAM) in their study. A hydraulic jump situation was investigated in both models. They used both experimental data and literature resources to evaluate the accuracy of both models. They stated that both models gave good results in this problem. Seyedashraf et al. (2017) investigated the shock waves and propagation of these waves by using artificial neural networks method. They used 5 different parameters as model channel length, upstream and downstream water heights, time and distance factors. He et al. (2017) investigated the flood wave in mobile and vegetative beds by means of a two-dimensional, depth-average numerical model. In addition, they conducted experiments and compared the results of numeric model and experiments. Hooshyaripor et al. (2017) designed an experimental setup with a 4.5-m-long 2.25-m-wide reservoir and a 9.3-m-long 0.51-m-wide downstream area. In this setup, they conducted experiments with different reservoir capacities and side slope conditions and examined the effect of these parameters on flood wave propagation. Ashraf et al. (2018) investigated the dam failure event, which occurred due to overtopping, statistically and experimentally. In order to estimate the collapse parameters, a regression analysis was performed based on the events that had occurred before. At the same time, five dams were tested on cohesive and non-cohesive soils. They concluded that the obtained equations and the results of the experiments carried out in non-cohesive soils were compatible with each other. Liu et al. (2018) established a physical model with a house in a horizontal rectangular channel 40 m long, 3.5 m wide and 0.4 m deep and examined the effect of the flood wave on the house. Yang et al. (2018) examined flood wave propagation by modelling dam break in FLOW-3D program. Issakhov et al. (2018) investigated the flow after the dam break using numerical analysis method by using the two- and three-dimensional Navier–Stokes equations. They compared the numeric model results with the experimental ones available in the literature. Munoz and Constantinescu (2018) used the RANS model, which utilized the VOF method to investigate the dam break currents. They compared the numerical results with those obtained from the experiments carried out in the laboratory. Wang et al. (2019) investigated experimentally the flood wave resulting from the dam break in triangular and rectangular channels. They carried out current measurements using the digital image processing method. They contributed to the understanding of the effect of wet downstream conditions on the flood wave. Khoshkonesh et al. (2019) examined the effect of the initial conditions such as reservoir water level, length and width of the reservoir on the flow that occurred after the dam broken. They determined the change in free water surface by using the VOF method. In numerical analysis, they compared the two models using Reynolds-averaged Navier–Stokes and LES turbulence models. Khoshkonesh et al. (2021) numerically evaluated the effects of partial dam break width on the flood wave. They used the VOF (volume of fluid) method to examine this dam break waves. The results were compared with the experimental results

available in the literature. They performed numerical analyses using different turbulence models and concluded that the best result was obtained with the LES model. Bahmanpouri et al., (2021) investigated the sediment transport that occurs as a result of dam failure experimentally and numerically. They carried out their experiments on a rectangular canal with a length of 5 m, a width of 0.16 m and a height of 0.4 m, with a vertical cover in the middle. They used three different sediment compaction rates in the downstream region. They used three different turbulence models in their numerical studies. Kocaman et al., (2021) investigated the tail water effect on dam break experimentally and numerically. Experiments were carried out in a rectangular channel with a length of 1.0 m, a width of 0.5 m and a height of 0.35 m. Three different tests were performed in dry and wet bed conditions at two different tailwater levels. The water levels were determined at five different points by using ultrasonic distance sensors (UDS). Flow-3D software were used to simulate the dam break. According to the results, it was revealed that there is a significant difference between the wave propagation in wet and dry bed conditions. They stated that the RANS model used in numerical studies was more compatible with the experimental results than the SWE model. Capasso et al., (2021) investigated the effect of the obstacle in the downstream region of the dam on the flood wave that occurs in case of dam break. Experiments were carried out in a rectangular channel with a length of 10 m, a width of 0.5 m and a height of 0.35 m. They placed a rectangular obstacle with a length of 0.15 m and a width of 0.08 m in the downstream region. They measured the water levels with ultrasonic sensors at five points. For numerical analysis, DualSPHysics model was used. According to the results, they stated that this program can be useful for simulating three-dimensional dam break models. Zuo et al. (2022) investigated the effect of dam break wave on solid wall using the mesh free method. Numerical analyses were performed at different initial water depths and wet bed conditions. They concluded that wet bed conditions at different depths would cause different flow patterns and free surface deformations. At the same time, they stated that the increase in tail water depth delayed the time to reach the maximum pressure value. Najar and Gül (2022) investigated the effects of dam break parameters on the flood hydrograph by means of HEC-RAS. Hazard maps were also obtained for different dam break scenarios. Ghaeini-Hessaroeyeh et al. (2022) developed a finite volume model based on shallow water equations to model the dam break flood wave. They compared their model results with experimental studies available in the literature, and they revealed that the model has good accuracy in modelling dam break flood wave.

Even though there are many researches on flood wave propagation caused by dam break, most of the experiments were carried out in a flume and dam break was simulated by removing a gate. Studies performed by means of a physical model are rare. In this study, the dam break experiments were carried out in the distorted physical model of the Urkmez Dam and at its downstream part also involving the vegetation. The horizontal and vertical scales are 1/150 and 1/30, respectively. The water depths and local velocities were measured by means of elaborated devices and the propagation of the flood wave was recorded by high-precision cameras. In addition, numerical analysis was achieved by using the FLOW-3D program. The results obtained from the numerical analysis were found to be in accord with the experimental findings.

2 Materials and Method

2.1 Physical Model

Experiments were carried out by using the distorted physical model of Urkmez Dam. Urkmez Dam is located on the Urkmez Stream, in the borders of the province of Izmir, Turkey. The dam is used for drinking water. The distorted physical model was constructed in Hydraulic Laboratory, Civil Engineering Department, Dokuz Eylul University (Fig. 1). The distorted physical model includes Urkmez Dam reservoir, dam body and downstream region including the residential area. The design and construction details of the distorted physical model were given by Guney et al. (2014). The horizontal and vertical scales of the distorted physical model are $L_{r,x} = L_{x,m}/L_{x,p} = 1/150$ and $L_{r,z} = L_{z,m}/L_{z,p} = 1/30$, respectively. $L_{x,m}$, $L_{x,p}$, $L_{z,m}$ and $L_{z,p}$ represent homologous lengths in the model and prototype in horizontal and vertical directions.

According to the Froude model simulation, Froude numbers ($Fr = \frac{V}{\sqrt{gL}}$) must be equal both at model and prototype.

Fig. 1 Urkmez Dam physical model

$$\frac{V_m}{\sqrt{g_m L_{m,z}}} = \frac{V_p}{\sqrt{g_p L_{p,z}}} \quad (1)$$

where V_m and V_p represent velocities of homologous points in the model and prototype, and g_m and g_p are gravitational accelerations in the model and prototype. According to Eq. 1, velocity and time scales are obtained as follows:

$$V_r = \frac{V_m}{V_p} = \sqrt{\frac{L_{m,z}}{L_{p,z}}} = L_{r,z}^{1/2} \quad (2)$$

$$T_r = \frac{T_m}{T_p} = \frac{L_{r,x}}{\sqrt{L_{r,z}}} = \frac{1}{m_d} L_{r,z}^{1/2} \quad (3)$$

where $m_d = L_{r,z} / L_{r,x}$ is the distortion coefficient. The characteristics of the prototype and the physical model are given in Table 1.

The vegetation cover at downstream part of the dam was determined by using satellite images and fieldwork. Plastic brushes were used as a vegetation cover at the downstream part of the physical model, and they were located at relevant places. The plastic brushes used in the downstream area are 8 cm high and 3 cm wide, and any deformation was observed in the plastic brushes during the experiments.

The partial dam break scenario was achieved by lifting the trapezoidal part of the dam body by means of a motor. The photographs of the dam break mechanism are given in Fig. 2.

2.2 Measurements

During the experiments, temporal variations of water depths and velocities were measured. UltraLab ULS (ultrasonic level sensor) 80-D device with USS20130 sensors was used to measure time-dependent depth at six points. The device has 8 channels allowing the simultaneous measurement of water depth at 8 different locations. The measurement range of the USS20130 sensor is between 200 and 1300 mm with a resolution of 0.18 mm. The sample rate and the frequency of the sensor are up to 75 Hz and 200 kHz, respectively. Since the sensors are mounted above the water surface, measurements can be taken without disturbing the flow. Time-dependent velocities were measured by using the Sontek MicroADV device at two points. The sampling rate of the MicroADV device is up to 50 Hz with a resolution of 0.01 cm/s. Kaolin clay was mixed in the reservoir with a ratio of 10% as suspended solid materials to increase the accuracy of the velocity measurements. The images of ULS 80-D device and MicroADV device measurement devices are shown in Fig. 3.

Table 1 Characteristics of the prototype and the physical model

Characteristic	Prototype	Model
High of dam (m)	32	1.07
Crest Length (m)	426	2.84
Crest Width(m)	12	0.08
Reservoir volume for minimum level (m^3)	375,000	0.556
Reservoir volume for maximum level (m^3)	8,625,000	12.78
Reservoir volume for normal level (m^3)	7,950,000	11.78
Active capacity (m^3)	7,575,000	11.22

Fig. 2 **a** Before dam break; **b** after dam break

3 Experimental Results

The experiments were performed for three different reservoir levels to investigate the effect of dam reservoir level on flood wave propagation. The features of the performed experiments are given in Table 2. During the experiments, water levels were measured at six different points (S2-S6) and velocities were measured at two different points (V1-V2). The locations and the coordinates of the measurement points are shown in Fig. 4.

Fig. 3 **a** ULS 80-D device and USS20130 sensors; **b** MicroADV device and probes

Table 2 The features of the performed experiments

Experiment No	Shape of the breach	Dam reservoir level (cm)
T98	Trapezoidal	98
T88	Trapezoidal	88
T80	Trapezoidal	80

To check the accuracy of the experiments, each experiment was repeated at least twice. The output hydrographs related to the experiments were obtained by means of the model reservoir water depth–volume curve that was predetermined from the calibration. The output hydrographs and temporal water depths are given in Fig. 5.

According to the results of the experiments, it is revealed that as the initial reservoir level decreases, the water depths measured during the propagation of the flood wave in the downstream region decrease and the time to reach the maximum water depth increases, as expected.

The maximum water depths were found to be nearly 22 cm, 19 cm and 16 cm at point S2 located on the right bank close to the dam body during the experiments T98, T88 and T80, respectively. These values correspond to 6.6 m, 5.7 m and 4.8 m in the prototype. The residential area in this region is sparse and considering the flood wave with a depth of 6.6 m, it can be said that the first two floors of the buildings will be flooded. The time to arrive to this point was measured as approximately 2 s for all experiments. When this value is transferred to the prototype by using distorted simulation model laws, the flood wave will reach this point in 54.8 s. The times to reach the maximum water level of the flood wave were 8 s, 8.2 s and 8.4 s for the experiments T98, T88 and T80, respectively. These values correspond to 3.65 min, 3.74 min and 3.84 min in the prototype, respectively.

The maximum water depths recorded at point S3 on the left bank were 10 cm, 4.65 cm and 4.6 cm for the experiments T98, T88 and T80, respectively. These values correspond to 3.0 m, 1.4 m and 1.38 m water depth in the prototype. The time to reach the maximum water level of the flood wave was similar for all experiments as 3 s, which corresponds to 1.37 min in the prototype.

The level meter S4 is located on the right bank in the middle of the downstream area and close to Urkmez Creek. The measured maximum water depths were 2.73 cm, 0.96 cm and 0.43 cm for the experiments T98, T88 and T80, respectively. These values correspond to 82 cm, 29 cm and 13 cm water depth in the prototype. The maximum water level was observed at 12th, 14.8th and 15th seconds, which corresponds to 5.48 min, 6.76 min and 6.85 min in nature.

The points S5 and S6 are located in the middle of the downstream area on the right and left bank, respectively. There is settlement area at the downstream part of the point S5, and the settlement area is more intense at point S6. The measured maximum water depths for S5 were 0.81 cm, 0.51 cm and 0.36 cm for the experiments T98, T88 and T80, respectively. These values correspond to 24.3 cm, 15.3 cm and 10.8 cm water depth in the prototype. The maximum water level was observed at 12.6th, 15.4th and

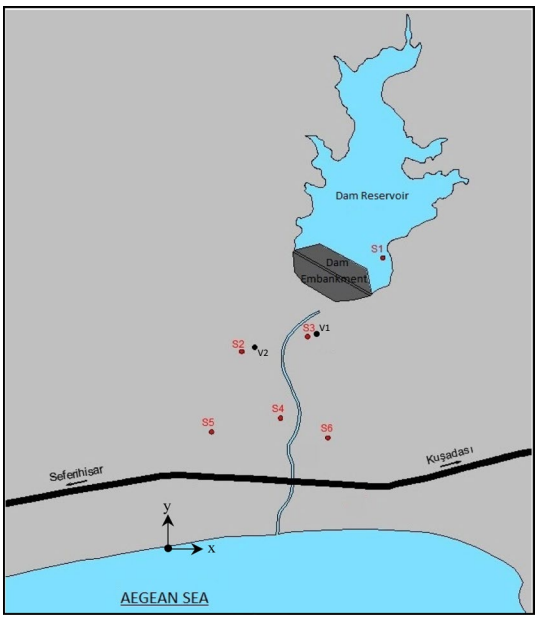

Fig. 4 Locations of measurement points at physical model

Measurement point	X (m)	Y (m)
V1	4.85	12.4
V2	3.81	11.45
S2	3.75	11.4
S3	4.78	12.42
S4	3.8	8.04
S5	0.53	7.93
S6	6.93	6.72

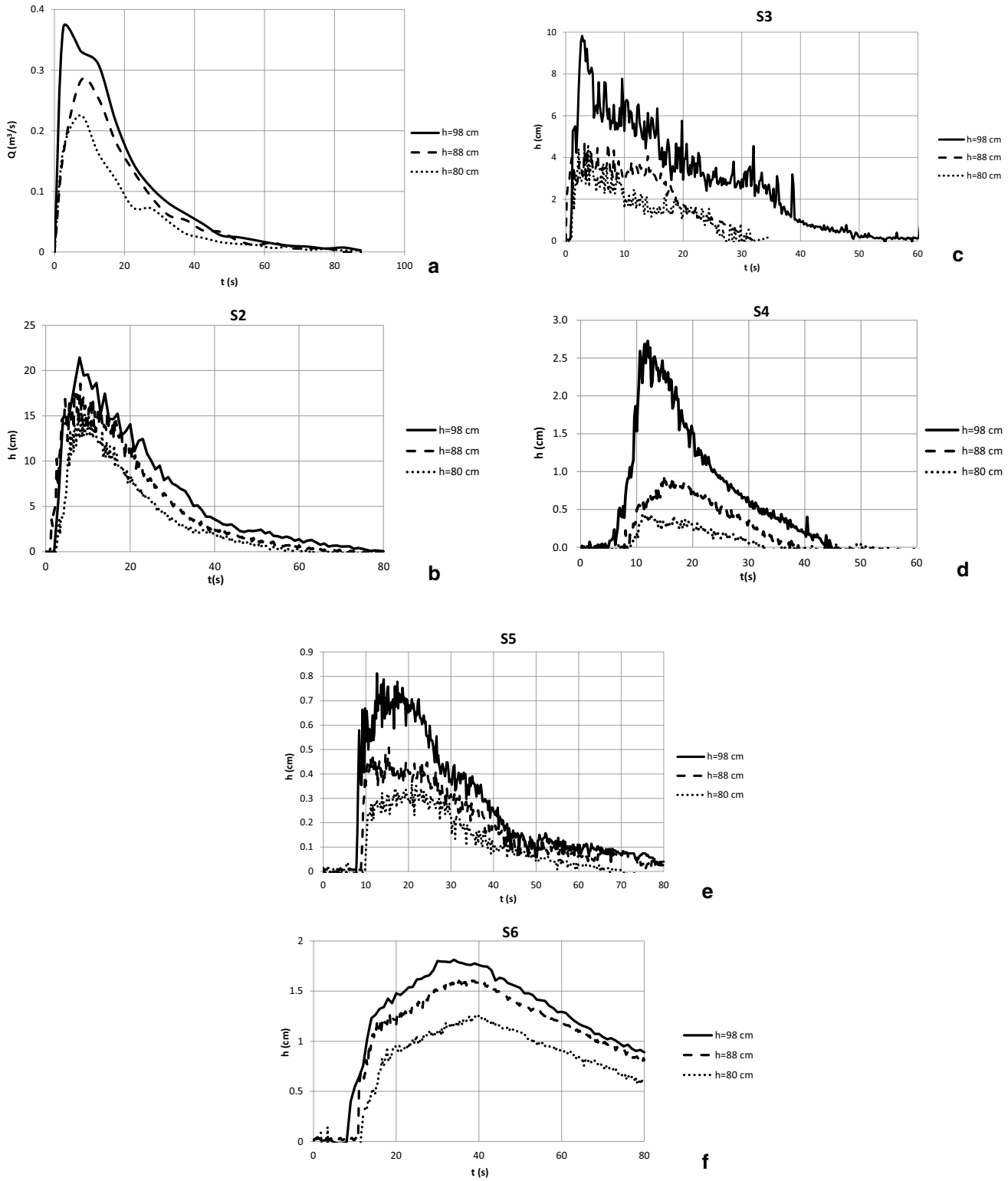

Fig. 5 **a** Output hydrographs *Q(t)* and temporal variation of water depths at measurement point, **b** S2, **c** S3, **d** S4, **e** S5, **f** S6

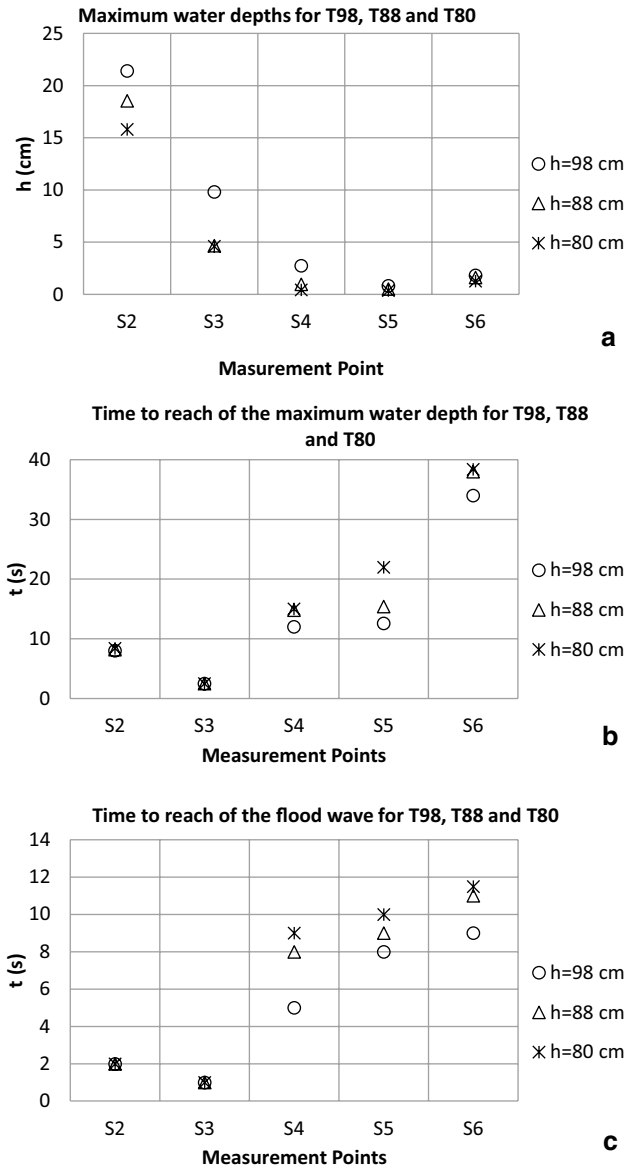

Fig. 6 **a** Maximum water depths, **b** time to reach of the maximum water depth, **c** time to reach of the flood wave

22nd seconds, which corresponds to 5.75 min, 7.03 min and 10.05 min in nature. The measured maximum water depths for S6 were 1.81 cm, 1.61 cm and 1.26 cm for the experiments T98, T88 and T80, respectively. These values correspond to 54.3 cm, 48.3 cm and 37.8 cm water depth in the prototype. The maximum water level was observed at 34th, 38th and 38.4th seconds, which corresponds to 15.53 min, 17.35 min and 17.54 min in nature.

The measured maximum water depths, time to reach of the maximum water depth and flood wave arrival times for the experiments T98, T88 and T80 are given in Fig. 6a, b and c, respectively.

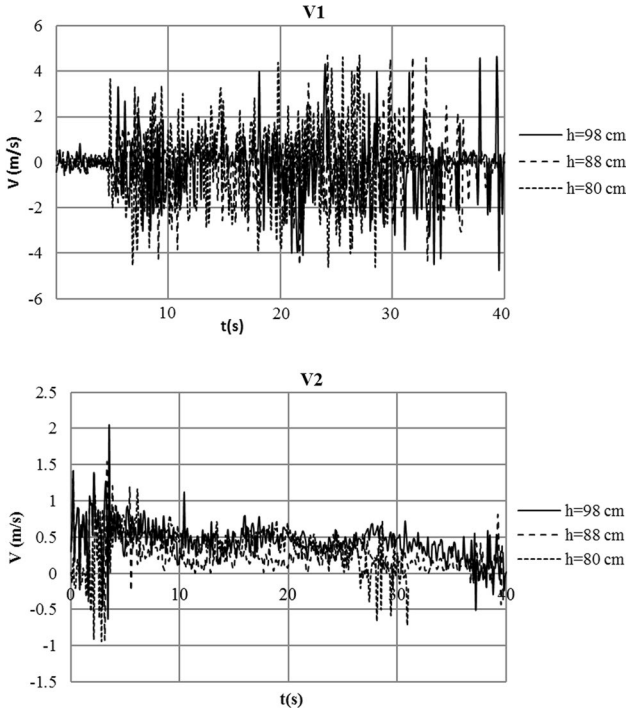

Fig. 7 Temporal variation of velocities at measurement points V1 and V2

In the experiments performed in the case of different water depths in the reservoir, the time-dependent flow velocities measured at points V1 and V2 are given in Fig. 7

It is seen that the time-dependent flow velocities at V2 measurement point are quite regular compared to the time-dependent flow velocity at V1 measurement point. The main reasons for this are the fact that the measurement point V1 is much closer to the dam body than V2, and the strong turbulences created by the high velocity flood current at the dam outlet at this point and the irregularities in the flow regime. The maximum velocities measured at the V2 measurement point for the T98, T88 and T80 experiments were 2.03 m/s, 1.53 m/s and 1.16 m/s, respectively. These maximum velocity values correspond to 11.12 m/s, 8.38 m/s and 6.36 m/s in the prototype. The mean velocities were 0.43 m/s, 0.26 m/s and 0.24 m/s for the experiments T98, T88 and T80, respectively. These velocity values correspond to 2.35 m/s, 1.42 m/s and 1.32 m/s in the prototype. These results show that the higher the reservoir level, the higher the maximum velocity at downstream part of the dam, as expected.

The propagation of the flood wave was recorded by means of high precision cameras. The images taken 3 s, 6 s, 10 s, 15 s, 25 s and 35 s after the start of the experiments T98, T88 and T80 are given in Figs. 8, 9 and 10, respectively. When the obtained images are examined, it is seen that as the dam lake level decreases, the time to reach the

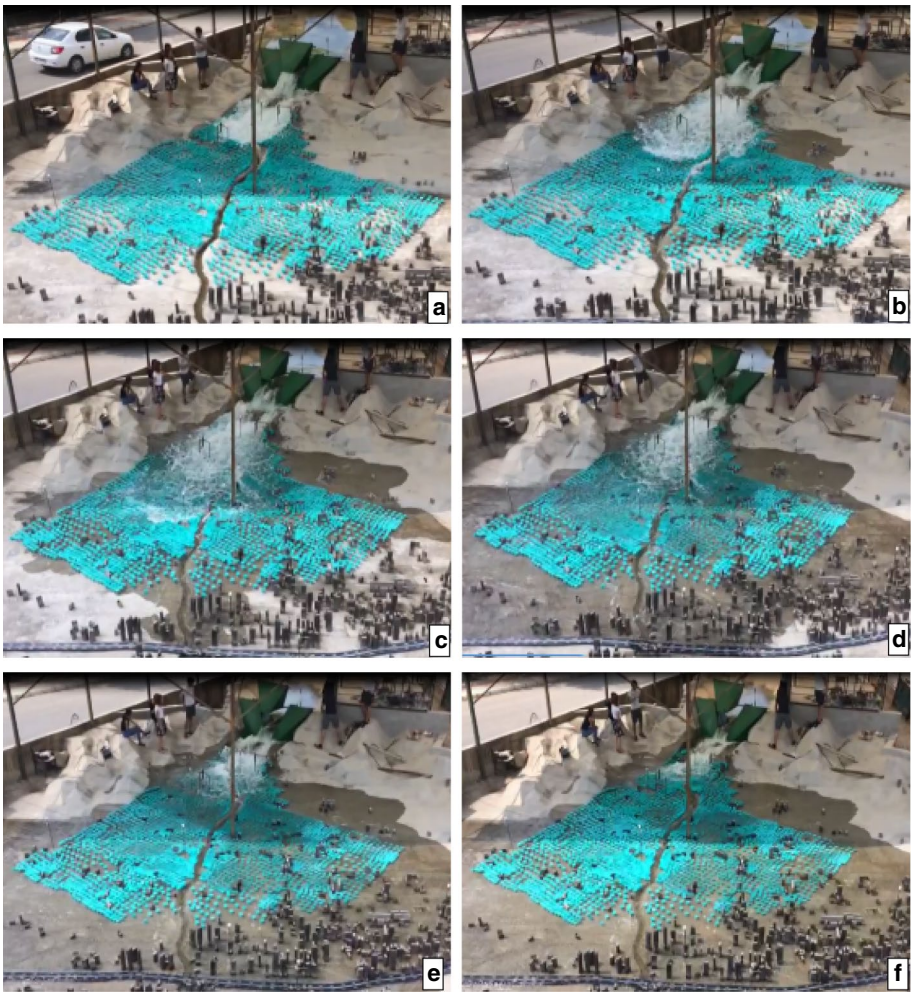

Fig. 8 The images taken at time [s], **a** 3, **b** 6, **c** 10, **d** 15, **e** 25, **f** 35 after the start of the experiment T98

measurement points of the flood increases and the spatial spread is delayed.

According to observations, it is observed that the spread of the flood wave in the downstream region is delayed as the initial level in the reservoir decreases. This finding, as expected, proves the accuracy of the experiments.

4 Numerical Model

In this study, the flood caused by the partial collapse of the dam with trapezoidal breach was numerically modelled for the physical model experiments by means of Flow-3D software. The purpose of the numerical model is to perform numerical simulations of different collapse scenarios. The most important process in numerical models is the calibration and verification of the numerical model.

Numerical modelling was carried out by using the Flow-3D software that includes advanced numerical techniques to solve time-dependent three-dimensional flow problems. Fluid motion is defined by nonlinear and time dependent second-order differential equations. The inertia of the gas adjacent to the liquid is neglected, and the volume occupied by the gas replaces the mass space represented by uniform pressure and temperature.

Three-dimensional motion (RANS: Reynolds-averaged Navier–Stokes) and continuity equations can be solved simultaneously in Flow-3D software by using finite volume method. Continuity and motion equations in Cartesian coordinates are given below (Flow science, 2007):

$$\frac{\partial}{\partial x_i}\left(u_i A_i\right) = 0 \tag{4}$$

$$\frac{\partial u_i}{\partial t} + \frac{1}{V_f}\left(u_j A_j \frac{\partial u_i}{\partial x_j}\right) = -\frac{1}{\rho}\frac{\partial p}{\partial x_i} + G_i + f_i \tag{5}$$

where u_i is the flow velocity in the direction i, A_j is the fractional area of the fluid in each cell, V_f is the volume fraction of the fluid in each cell, p is pressure, G_i is the body acceleration in the direction i, and f_i is the viscous acceleration in the direction i.

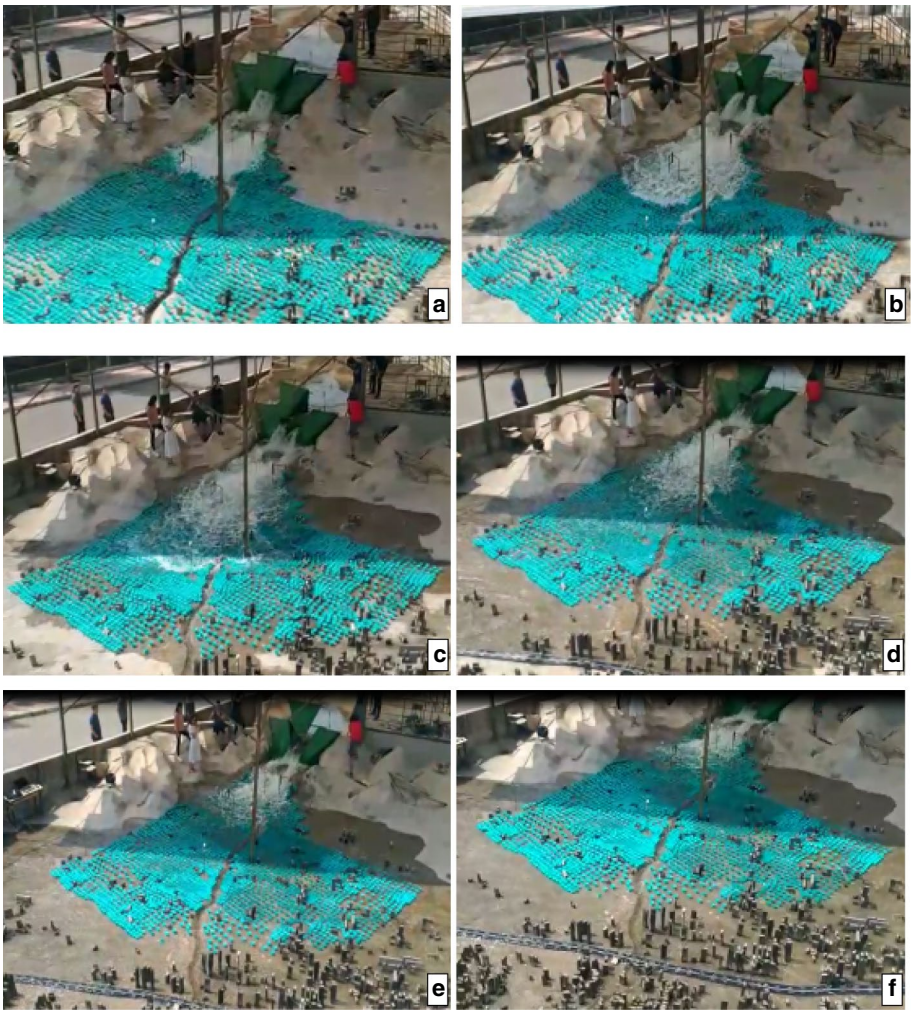

Fig. 9 The images taken at time [s], **a** 3, **b** 6, **c** 10, **d** 15, **e** 25, **f** 35 after the start of the experiment T88

The solution network consists of rectangular elements, and fluid properties (pressure, viscosity, density …) are located in the centre of the rectangular elements, while flow properties (u, v, w) are taken into account on the surface of the elements.

The software determines how much of a cell occupies an obstacle by means of FAVOR (fractional area/volume obstacle representation) method. The value is zero if the cell is completely filled with an obstacle or it is completely empty. If a cell is partially filled with fluid, this value takes between zero and one, depending on the percentage. Fluid volume (VOF; volume of fluid) method is used in the software to determine free surfaces. In this method, as in the FAVOR method, the volume of fluid in the cell is determined. The volume of fluid (VOF) method in FLOW-3D consists of three main components such as the definition of the volume of fluid function, a method to solve the VOF transport equation and setting the boundary conditions at the free surface.

This software includes different turbulence approaches such as two-equation k–ε model, Prandtl mixing length model, turbulent energy, two equation k–ω model, RNG (renormalized group) and LES (large-eddy Simulation). In this study, two-equation k–ε and k–ω models, RNG (renormalized group) and LES (large eddy simulation) were used. The two equation models (k–ε) calculate both the turbulence kinetic energy (k) and the dissipation rate (ε). It is commonly used to simulate mean flow characteristics for turbulent flow conditions. The two-equation k–ω models calculate turbulence kinetic energy (k) and specific rate of dissipation (ω), and it is used in free shear flows. The RNG model derives a turbulence model similar to the k–ε model and provides better solutions for wall heat transfer, mass transfer and curving flows. Large eddy simulation—LES—solves most turbulent fluctuations directly rather than using scalars to represent the average turbulent kinetic energy (Flow science, 2007).

The physical model of the dam was defined in two different ways in the Flow-3D software. First, the numerical model of only the downstream section of the dam was generated, and then the second numerical model was generated by including the reservoir. Both numerical models are given in Fig. 11a and b, respectively. Wall (no-flow) and

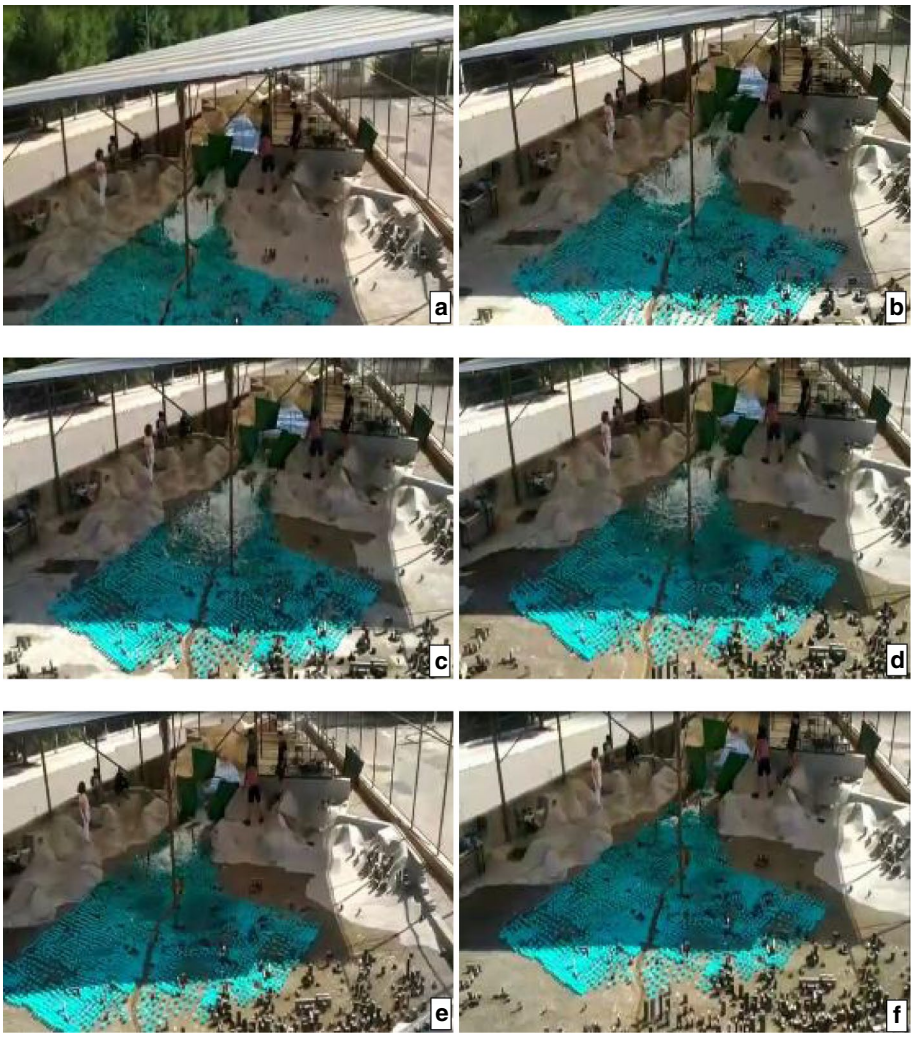

Fig. 10 The images taken at time [s], **a** 3, **b** 6, **c** 10, **d** 15, **e** 25, **f** 35 after the start of the experiment T80

atmospheric pressure was determined as boundary conditions for the ground of the model and air–water interface, respectively. The other boundary conditions set as outflow. The numerical models were performed for different mesh sizes such as 5*5 cm, 3.5*3.5 cm, 2.5*2.5 cm and 2*2 cm. While it was observed significant differences between the results of 5*5 cm, 3.5*3.5 cm, 2.5*2.5 cm mesh sizes, these differences were not observed between 2.5*2.5 cm and 2*2 cm mesh sizes. So the mesh size of 2.5*2.5 cm obtained as the optimum mesh size. Hence, the solution area was divided into cells with a width of 2.5 cm, length of 2.5 cm and a height of 0.25 cm and a grid system was generated for numerical analysis. The grid system consists of 2,688,000 for the model.

First, the hydrograph obtained from the experimental studies was defined as boundary condition for the numerical model. While numerical solutions were carried out by using different turbulence models with this boundary condition, on the other hand, a numerical model of the dam lake was generated. For the trapezoidal collapse of the dam, a moving object was defined in the numerical model as shown in Fig. 12. By defining a velocity in the + z direction for the moving object, the partial dam break scenario was simulated according to the related experiments.

The features of the performed numerical models are given in Table 3.

Comparison of measured and computed water depths is given in Figs. 13, 14 and 15 for the experiments T98, T88 and T80, respectively.

The numerical models were simulated by using four different turbulence models while keeping the boundary condition constant as the hydrograph. According to the numerical results, it is seen that there is not a significant difference between the values obtained from different turbulence models. This result is compatible with those obtained by

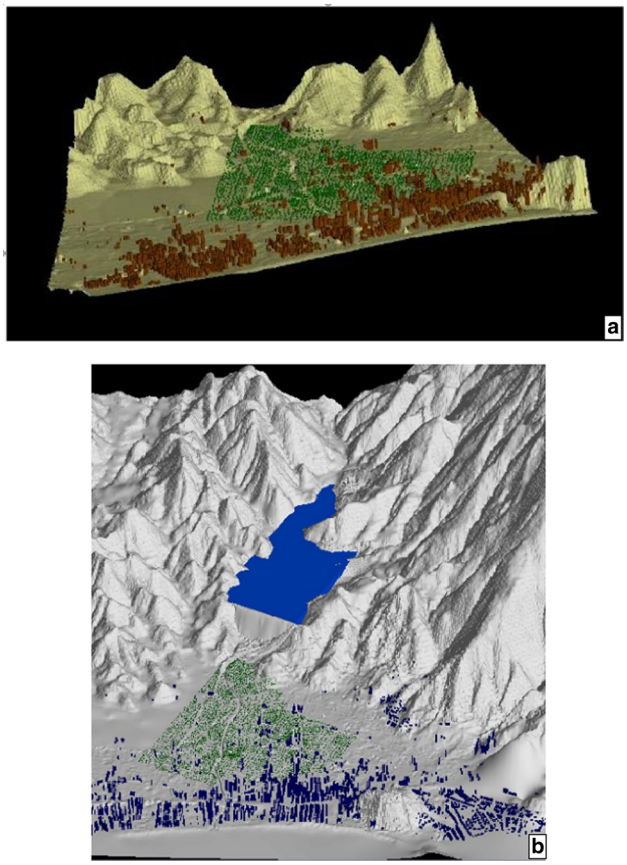

Fig. 11 Dam physical model transferred to Flow-3D software: **a** dam downstream topography only, **b** dam physical model with reservoir included

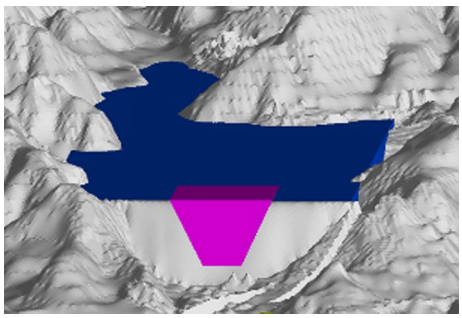

Fig. 12 Trapezoidal moving object image defined in the numerical model

Bahmanpouri et al. (2021) that the numerical models were simulated by using RNG, k–ε and k–ω turbulence models.

When the numerical model results are compared with the experimental ones, it is revealed that numerical models overestimate for all turbulence models when the boundary condition was the hydrograph. Besides, the numerical results

Table 3 The features of the performed numerical models

Simulation No	Dam Reservoir Level (cm)	Turbulence Model	Boundary Condition
T98-1	98	RNG	Hydrograph
T98-2	98	k–ε	Hydrograph
T98-3	98	K–ω	Hydrograph
T98-4	98	LES	Hydrograph
T98-5	98	RNG	Dam Reservoir
T88-1	88	RNG	Hydrograph
T88-2	88	K–ε	Hydrograph
T88-3	88	K–ω	Hydrograph
T88-4	88	LES	Hydrograph
T88-5	88	RNG	Dam Reservoir
T80-1	80	RNG	Hydrograph
T80-2	80	K–ε	Hydrograph
T80-3	80	K–ω	Hydrograph
T80-4	80	LES	Hydrograph
T80-5	80	RNG	Dam Reservoir

are in good agreement with those obtained from experiments when the dam lake is defined instead of hydrograph as a boundary condition. In this case, one can say that numerical model is more sensitive to the boundary condition than the turbulence model. It is also revealed that the performance of the three-dimensional numerical model depends on the mesh resolution. As stated already, once the mesh sizes get smaller, the solution time and computational capacity get increase. These results are also compatible with the study given by Khoshkonesh et al. (2021).

The results of the numerical model were evaluated in terms of determination coefficient (R^2) and scatter index (SI). These parameters are defined as follows:

$$R^2 = \frac{\text{SSR}}{\text{SSR} + \text{SSE}} \tag{6}$$

$$\text{SSE} = \sum_{i=1}^{n} \left(Y_i - \hat{Y}_i\right)^2 \tag{7}$$

$$\text{SSR} = \sum_{i=1}^{n} \left(\hat{Y}_i - \overline{Y}\right)^2 \tag{8}$$

$$\text{SI} = \frac{\sqrt{\frac{\text{SSE}}{n}}}{\overline{Y}} \tag{9}$$

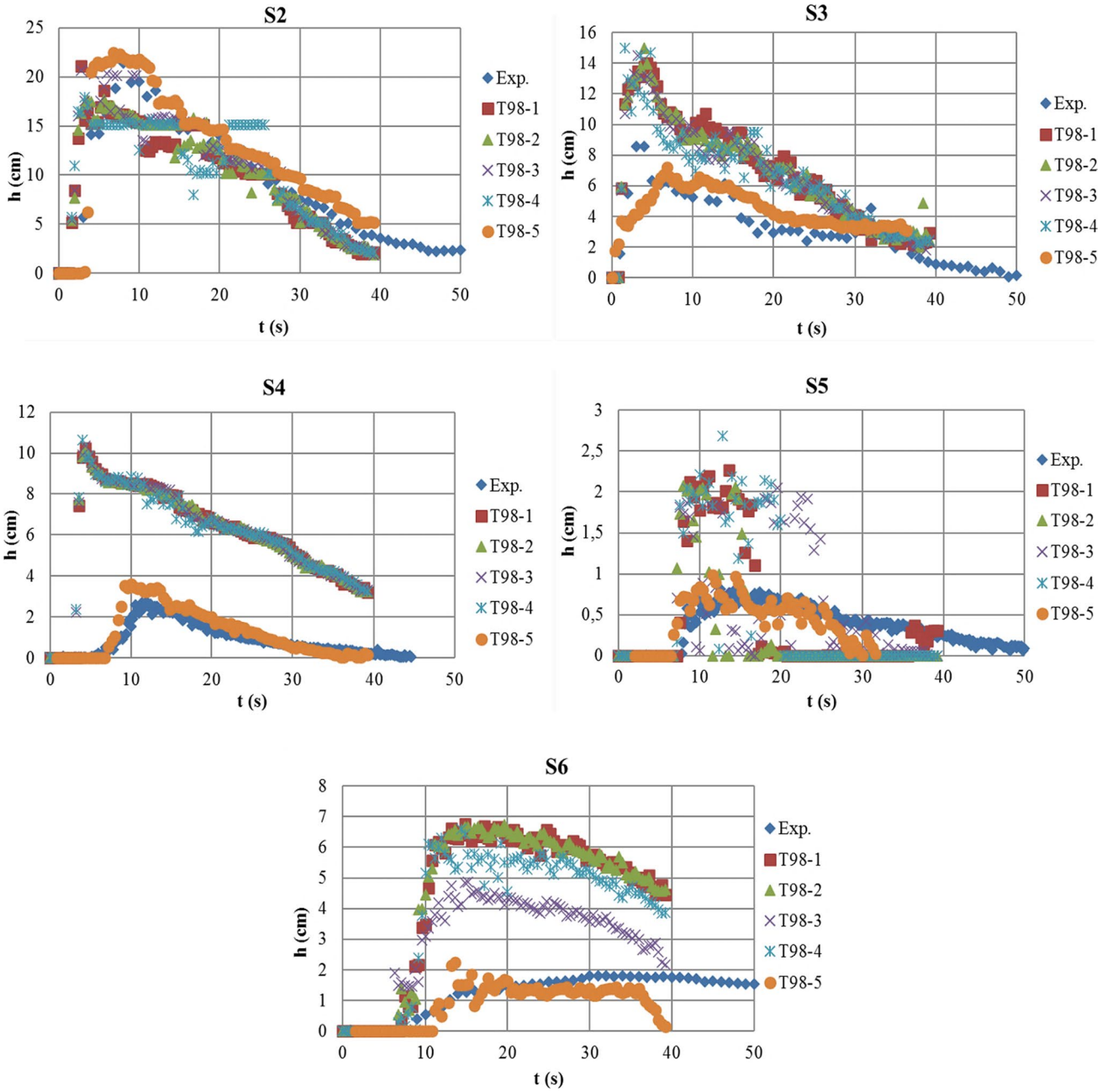

Fig. 13 Comparison of measured and computed water depths for the experiment T98

where n is the number of the data, Y_i is the experimental values, and $\widehat{Y}_i$ and $\overline{Y}$ are the values computed values and the mean value of the experimental data, respectively.

The scatter diagram including the measured values and those computed by Flow-3D is given in Fig. 16 for the experiment T98. The determination coefficient and scatter index values are given in Table 4.

When the numerical model results are compared with the experimental findings, it is seen that the water depths obtained in the case of dam reservoir boundary condition are more compatible with the experimental findings. It is also seen that the use of different turbulence models does not have a significant effect on the numerical results.

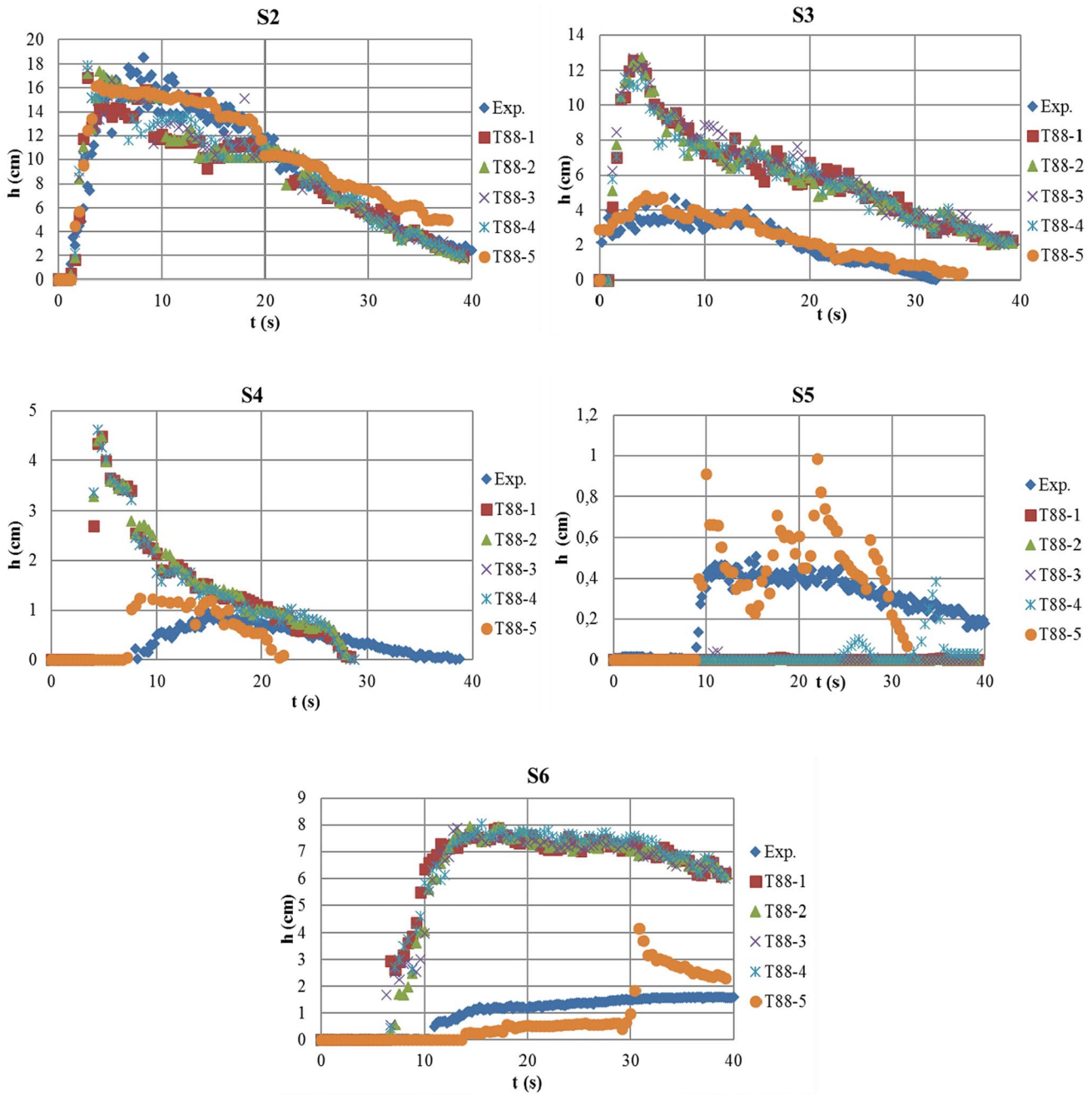

Fig. 14 Comparison of measured and computed water depths for the experiment T88

5 Conclusion

In this study, the dam break experiments were carried out in the distorted physical model of the Urkmez Dam and at its downstream part involving also the vegetation. According to the results of the experiments, it is revealed that as the reservoir level decreases, the water depths measured during the propagation of the flood wave in the downstream region decrease and the time to reach the maximum water depth increases, as expected. In areas where settlements are sparse in prototype, the maximum water depth was observed as 6.6 m and this depth was reached after 54.8 s of dam break so it can be said that the first two floors of the buildings will be flooded. In areas where settlements are intense in prototype, the maximum water depth was observed as 82 cm and this depth was reached after 5.48 min of dam break.

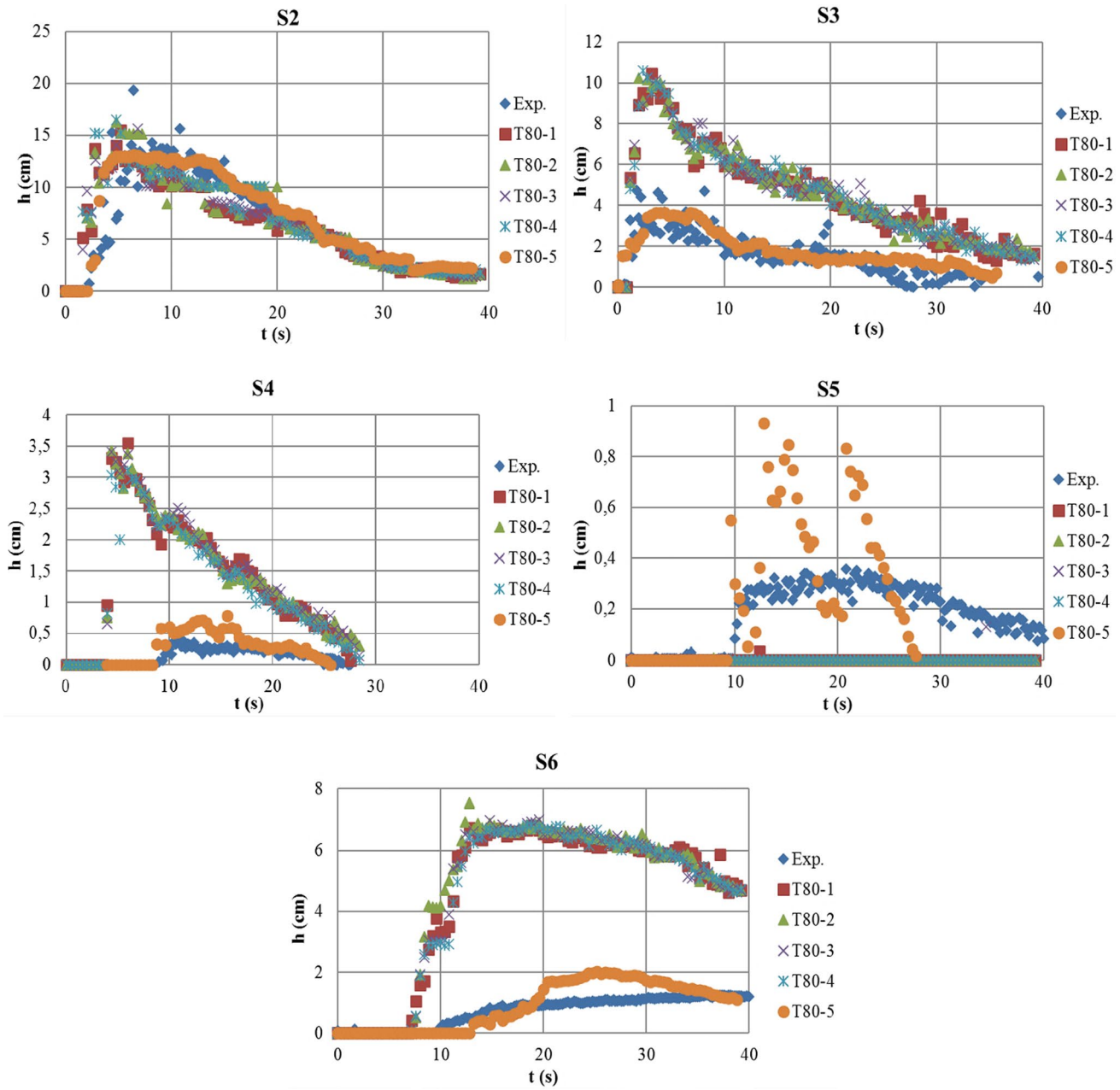

Fig. 15 Comparison of measured and computed water depths for the experiment T80

Experimental findings contain useful information for decision makers, especially to be used in early warning systems and emergency action plans, as they enable to predict kinematic parameters such as depth, time and velocity of the flood wave caused by dam break. Numerical model studies were also carried out within the scope of this study. For this purpose, Flow-3D, one of the advanced computational fluid dynamics software, was used. In the numerical model, three-dimensional basic equations with different turbulence models are solved with the finite volume technique. Two different boundary conditions were defined such as the output hydrographs obtained from experiments and dam reservoir. It was seen that the numerical model results were in much better agreement with the experimental data when the dam reservoir was used as boundary condition. By defining the

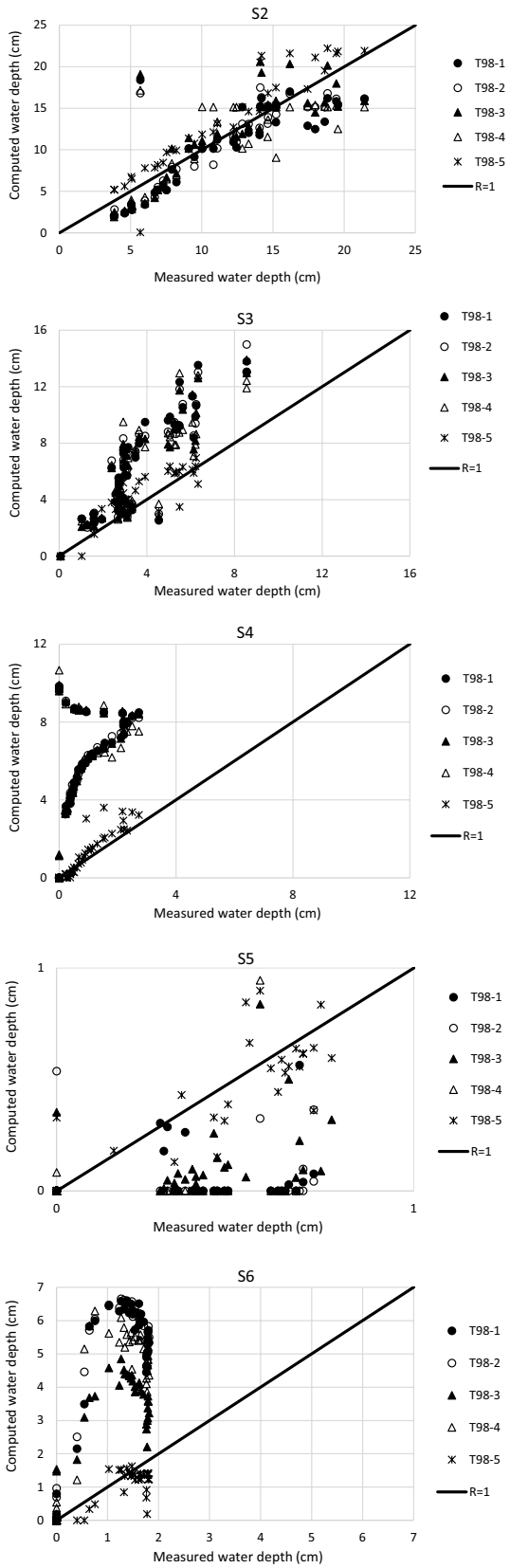

Fig. 16 The scatter diagram including the measured and computed values

Table 4 Determination coefficient and scatter index values

Simulation No	Measurement Point	SI	R^2
T98-1	S2	0.31	0.72
T98-2	S2	0.27	0.77
T98-3	S2	0.32	0.75
T98-4	S2	0.35	0.66
T98-5	S2	0.23	0.88
T98-1	S3	0.95	0.62
T98-2	S3	0.94	0.62
T98-3	S3	0.87	0.63
T98-4	S3	0.83	0.62
T98-5	S3	0.56	0.84
T98-1	S4	5.87	0.51
T98-2	S4	5.88	0.51
T98-3	S4	5.87	0.51
T98-4	S4	5.88	0.51
T98-5	S4	0.64	0.88
T98-1	S5	1.80	0.53
T98-2	S5	1.67	0.50
T98-3	S5	1.46	0.55
T98-4	S5	1.97	0.56
T98-5	S5	0.63	0.65
T98-1	S6	3.43	0.54
T98-2	S6	3.48	0.54
T98-3	S6	1.93	0.56
T98-4	S6	2.97	0.54
T98-5	S6	0.40	0.70

most suitable parameters and boundary conditions for the numerical model, different scenarios that cannot be generated in experimental studies can be tested through the numerical model.

Acknowledgements The authors thank to the Scientific and Technological Research Council of Turkey (TUBITAK) for supporting the study through the project 116M237.

Data Availability The data that support the findings of this study are available from the corresponding author (Semire Oğuzhan Güven), upon reasonable request.

References

Ashraf M, Soliman AH, El-Ghorab E, Zawahry AE (2018) Assessment of embankment dams breaching using large scale physical modeling and statistical methods. Water Sci 32:362–379. https://doi.org/10.1016/J.WSJ.2018.05.002

Bahmanpouri F, Daliri M, Khoshkonesh A, Namin MM, Buccino M (2021) Bed compaction effect on dam break flow over erodible bed; experimental and numerical modeling. J Hydrol 594:125645. https://doi.org/10.1016/j.jhydrol.2020.125645

Bayon A, Valero D, García-Bartual R, Jos F, Es-Mor V, Amparo L, Opez-Jim Enez P (2016) Performance assessment of OpenFOAM

and FLOW-3D in the numerical modeling of a low Reynolds number hydraulic jump. Environ Modell Softw. https://doi.org/10.1016/j.envsoft.2016.02.018

Capasso S, Tagliafierro B, Güzel H, Yilmaz A, Dal K, Kocaman S, Evangelista S (2021) A numerical validation of 3D experimental dam-break wave interaction with a sharp obstacle using Dual-SPHysics. Water 13(15):2133

Elkholy M, Larocque LA, Chaudhry MH, Imran J (2016) Experimental investigations of partial-breach dam-break flows. J Hydraul Eng 142:1–12. https://doi.org/10.1061/(ASCE)HY.1943-7900.0001185

Erpicum S, Dewals BJ, Archambeau P, Pirotton M (2010) Dam break flow computation based on an efficient flux vector splitting. J Comput Appl Math 234:2143–2151. https://doi.org/10.1016/j.cam.2009.08.110

Flow Science Inc. (2007). What's New in FLOW-3D Version 10.0. Flow 3D User's Manual. Santa Fe, New Mexico

Froehlich DC (2008) Embankment dam breach parameters and their uncertainties. J Hydraul Eng. https://doi.org/10.1061/ASCE0733-94292008134:121708

Ghaeini-Hessaroeyeh M, Namin MM, Fadaei-Kermani E (2022) 2-D dam-break flow modeling based on weighted average flux method. Iran J Sci Technol Trans Civil Eng 46(2):1515–1525

Güney MS, Tayfur G, Bombar G, Elci S (2014) Distorted physical model to study sudden partial dam break flows in an urban area. J Hydraul Eng 140:05014006. https://doi.org/10.1061/(ASCE)HY.1943-7900.0000926

Haltas I, Tayfur G, Elci S (2016) Two-dimensional numerical modeling of flood wave propagation in an urban area due to Urkmez dam-break, İzmir, Turkey. Nat Hazards. https://doi.org/10.1007/s11069-016-2175-6

He Z, Wu T, Weng H, Hu P, Wu G (2017) Numerical simulation of dam-break flow and bed change considering the vegetation effects. Int J Sediment Res 32:105–120. https://doi.org/10.1016/j.ijsrc.2015.04.004

Hooshyaripor F, Tahershamsi A, Razi S (2017) Dam break flood wave under different reservoir's capacities and lengths. Sadhana - Acad Proc Eng Sci 42:1557–1569. https://doi.org/10.1007/s12046-017-0693-x

Issakhov A, Zhandaulet Y, Nogaeva A (2018) Numerical simulation of dam break flow for various forms of the obstacle by VOF method. Int J Multiph Flow 109:191–206. https://doi.org/10.1016/j.ijmultiphaseflow.2018.08.003

Jeong W, Yoon JS, Cho YS (2012) Numerical study on effects of building groups on dam-break flow in urban areas. J Hydro-Environ Res. https://doi.org/10.1016/j.jher.2012.01.001

Khoshkonesh A, Nsom B, Gohari S, Banejad H (2019) A comprehensive study on dam-break flow over dry and wet beds. Ocean Eng 188:106279. https://doi.org/10.1016/j.oceaneng.2019.106279

Khoshkonesh A, Nsom B, Bahmanpouri F, Dehrashid FA, Adeli A (2021) Numerical study of the dynamics and structure of a partial dam-break flow using the VOF method. Water Resour Manag 35:1513–1528. https://doi.org/10.1007/s11269-021-02799-2

Kocaman S, Evangelista S, Guzel H, Dal K, Yilmaz A, Viccione G (2021) Experimental and numerical investigation of 3d dam-break wave propagation in an enclosed domain with dry and wet bottom. Appl Sci 11(12):5638

Lauber G, Hager WH (1998) Experiments to dambreak wave: horizontal channel. J Hydraul Res 36:291–306. https://doi.org/10.1080/00221689809498620

Liu L, Sun J, Lin B, Lu L (2018) Building performance in dam-break flow–an experimental study. Urban Water J 15:251–258. https://doi.org/10.1080/1573062X.2018.1433862

Munoz DH, Constantinescu G (2018) A fully 3-D numerical model to predict flood wave propagation and assess efficiency of flood protection measures. Adv Water Resour 122:148–165

Najar M, Gül A (2022) Investigating the influence of dam-breach parameters on dam-break connected flood hydrograph. Teknik Dergi. https://doi.org/10.18400/tekderg.796334

Ozmen-Cagatay H, Kocaman S (2010) Dam-break flows during initial stage using SWE and RANS approaches. J Hydraul Res 48:603–611. https://doi.org/10.1080/00221686.2010.507342

Ozmen-Cagatay H, Kocaman S, Guzel H (2014) Investigation of dam-break flood waves in a dry channel with a hump. J Hydro-Environ Res 8:304–315. https://doi.org/10.1016/j.jher.2014.01.005

Seyedashraf O, Rezaei A, Akhtari AA (2017) Dam break flow solution using artificial neural network. Ocean Eng 142:125–132. https://doi.org/10.1016/j.oceaneng.2017.07.002

Soares-Frazão S (2007) Experiments of dam-break wave over a triangular bottom sill. J Hydraul Res 45:19–26. https://doi.org/10.1080/00221686.2007.9521829

Soares-Frazão S, Zech Y (2008) Dam-break flow through an idealised city. J Hydraul Res 46:648–658. https://doi.org/10.3826/jhr.2008.3164

Wang B, Zhang J, Chen Y, Peng Y, Liu X, Liu W (2019) Comparison of measured dam-break flood waves in triangular and rectangular channels. J Hydrol 575:690–703. https://doi.org/10.1016/j.jhydrol.2019.05.081

Wood A, Wang KH (2015) Modeling dam-break flows in channels with 90 degree bend using an alternating-direction implicit based curvilinear hydrodynamic solver. Comput Fluids 114:254–264. https://doi.org/10.1016/j.compfluid.2015.03.011

Yang S, Yang W, Qin S, Li Q, Yang B (2018) Numerical study on characteristics of dam-break wave. Ocean Eng. https://doi.org/10.1016/j.oceaneng.2018.04.011

Zuo J, Xu T, Zhu DZ, Gu H (2022) Impact pressure of dam-break waves on a vertical wall with various downstream conditions by an explicit mesh-free method. Ocean Eng 256:111569